OPEN BIOLOGY

royalsocietypublishing.org/journal/rsob

Research

Cite this article: Zahm JA, Jenni S, Harrison SC. 2023 Structure of the Ndc80 complex and its interactions at the yeast kinetochore–microtubule interface. *Open Biol.* **13**: 220378. https://doi.org/10.1098/rsob.220378

Received: 23 December 2022
Accepted: 8 February 2023

Subject Area:
structural biology/cellular biology

Keywords:
cell division, chromosome segregation, kinetochore, Ndc80 complex, Dam1 complex, structure prediction

Author for correspondence:
Stephen C. Harrison
e-mail: harrison@crystal.harvard.edu

†These authors contributed equally to this study.

Electronic supplementary material is available online at https://doi.org/10.6084/m9.figshare.c.6431801.

THE ROYAL SOCIETY PUBLISHING

Structure of the Ndc80 complex and its interactions at the yeast kinetochore–microtubule interface

Jacob A. Zahm[1,†], Simon Jenni[1,†] and Stephen C. Harrison[1,2]

[1]Department of Biological Chemistry and Molecular Pharmacology, and [2]Howard Hughes Medical Institute, Harvard Medical School, Boston, MA 02115, USA

JAZ, 0000-0002-9600-5433; SJ, 0000-0001-5722-5890; SCH, 0000-0001-7215-9393

The conserved Ndc80 kinetochore complex, Ndc80c, is the principal link between mitotic spindle microtubules and centromere-associated proteins. We used AlphaFold 2 (AF2) to obtain predictions of the Ndc80 'loop' structure and of the Ndc80 : Nuf2 globular head domains that interact with the Dam1 subunit of the heterodecameric DASH/Dam1 complex (Dam1c). The predictions guided design of crystallizable constructs, with structures close to the predicted ones. The Ndc80 'loop' is a stiff, α-helical 'switchback' structure; AF2 predictions and positions of preferential cleavage sites indicate that flexibility within the long Ndc80c rod occurs instead at a hinge closer to the globular head. Conserved stretches of the Dam1 C terminus bind Ndc80c such that phosphorylation of Dam1 serine residues 257, 265 and 292 by the mitotic kinase Ipl1/Aurora B can release this contact during error correction of mis-attached kinetochores. We integrate the structural results presented here into our current molecular model of the kinetochore–microtubule interface. The model illustrates how multiple interactions between Ndc80c, DASH/Dam1c and the microtubule lattice stabilize kinetochore attachments.

1. Introduction

Kinetochores, essential components of the chromosome segregation machinery, connect centromeres to the mitotic spindle. The bridge between centromere-associated kinetochore assemblies and spindle microtubules is the Ndc80 complex (Ndc80c), a heterotetramer, conserved from yeast to mammals, with globular elements at both ends of an approximately 600 Å long, largely α-helical coiled-coil shaft (figure 1) [2–4]. Closely paired calponin homology (CH) domains of Ndc80 and Nuf2 at one end, augmented by a flexible, N-terminal extension of Ndc80, form a microtubule-attachment module [5–7]. Tightly associated RWD domains of Spc24 and Spc25 at the other end bind adaptor proteins emanating from centromere-bound, kinetochore components [8–11]. The coiled-coil shaft of Ndc80 : Nuf2 has two specializations—a kink or hinge at about 160 Å from the globular end [3] and a so-called 'loop' at about 240 Å. The latter structure is effectively an insertion of approximately 50–80 residues into Ndc80 opposite a continuous helix in Nuf2 [12]. The shafts of the two heterodimeric components—Ndc80 : Nuf2 and Spc24 : Spc25—meet in an overlapping, four-way junction, or tetramerization domain, included in the crystal structure of a shortened, 'dwarf' Ndc80c [13].

In yeast, several additional kinetochore components bind at various positions along the Ndc80c. At least three interactions involve subunits of the DASH/Dam1 complex (Dam1c, consisting of Ask1, Dad1, Dad2, Dad3, Dad4, Dam1, Duo1, Hsk3, Spc19 and Spc34) [14–16], which coordinates end-on attachment of multiple Ndc80c rods around the splayed plus end of a kinetochore microtubule [17]. A fourth contacting component is the microtubule polymerase, Stu2 [18]. Figure 1 shows positions of the DASH/Dam1c interactions, as mapped by genetic and

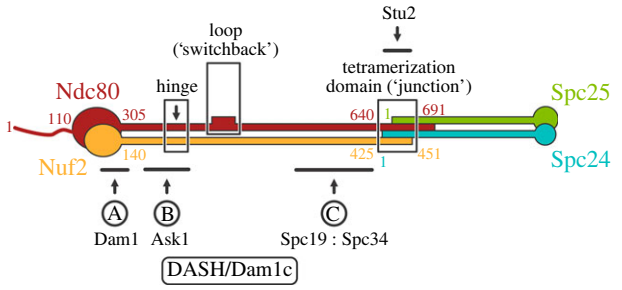

Figure 1. Schematic diagram of Ndc80c. Residue numbers for key junction points in the *S. cerevisiae* sequences shown. Solid ovals represent the CH domains of Ndc80 (red) and Nuf2 (orange) at one end and the RWD domains of Spc24 (blue) and Spc25 (green) at the other. The positions of the Ndc80c hinge, loop and the four-way junction are boxed and labelled, respectively. The locations of the three interactions, defined by cross-linking mass spectrometry [1], between Ndc80c and C-terminal extensions of DASH/Dam1c subunits are indicated. The interaction of Stu2 with the tetramerization domain is also indicated. Interaction A involves Dam1, interaction B, Ask1 and interactions C, Spc19 : Spc34.

biochemical studies including mass spectrometric analysis of cross-linked peptides [1,17,19]. The Dam1 subunit binds at the base of the Ndc80 : Nuf2 globular 'head', Ask1 along the shaft between the globular head and the hinge, and Spc19 : Spc34 between the loop and the four-way junction, respectively. All these interactions between Ndc80c and DASH/Dam1c are regulated by phosphorylation of certain serine or threonine residues [19,20]. The Stu2 interaction, visualized by X-ray crystallography, is with the four-way junction [21].

Budding yeast kinetochores first attach to the lateral surface of spindle microtubules [22]. This initial capture must convert to end-on attachment to produce a structure that can track with microtubule shortening and bear the load thereby generated [23,24]. The conversion occurs when the end of a disassembling microtubule reaches the laterally attached kinetochore [22,25,26]. The DASH/Dam1c ring is dispensable for lateral capture but essential for conversion to end-on capture [26]. Deletions and certain mutations in the Ndc80 loop block this conversion [27]. The microtubule polymerase, Stu2, also appears to have a role [18,26]. As steps towards working out the molecular events in conversion from lateral to end-on attachment, we have extended our previous studies of the Stu2 interaction at the Ndc80c four-way junction [21] by determining crystal structures of the Ndc80 loop and of the Dam1 association at the base of the Ndc80 : Nuf2 globular head. The latter structure explains why phosphorylation of Dam1 serine residues 257, 265 and 292 by Ipl1/AuroraB inhibits attachment [20,28–31]. We compare the new structures with the AlphaFold 2 (AF2) [32] predictions that motivated design of the constructs we used. We also show that the AF2 prediction of the Ndc80c's hinge point agrees with the position of selective proteolytic sensitivity described in our early studies of Ndc80c architecture [2].

2. Results

2.1. The Ndc80 loop region is a rigid switchback structure

Ndc80 amino acid sequences across the region that contains the loop align well for a set of budding yeasts (figure 2*a*) and also for a representative set of metazoans (figure 2*b*), but the sequences align poorly between those two groups (electronic supplementary material, data S1–S4). Structure predictions from multi-chain AF2 for segments of Ndc80 : Nuf2 that include the loop and flanking sequences are thus, as expected, very similar across the budding yeasts and across metazoans, and overall quite similar between those two groups, but distinct in some local features (figure 2*c*). An essentially identical prediction has motivated recent functional studies for the human Ndc80 loop by another group, as discussed at the end of this paper [33]. Both sequences and predicted structures for fission yeast (*Schizosaccharomyces pombe*) and fungi in families other than *Saccharomycetaceae* align, in predicted structure and in sequence, with the metazoans (figure 2*b* and *c*). We expressed segments of both the yeast and human Ndc80 polypeptide chains and the respective paired segments (from the prediction) of Nuf2. We obtained crystals of the human complex in space group C_2 ($a = 49.9$ Å, $b = 72.3$ Å, $c = 80.1$ Å, $\beta = 98.56°$). From merged datasets that extended to a minimum Bragg spacing of 2.0 Å, we determined the structure by molecular replacement with a four-part model based on the AF2 prediction (see Materials and Methods for details and for controls to eliminate model bias, electronic supplementary material, table S1 for data and refinement statistics, and electronic supplementary material, figure S1 for representative density maps). The final model (figure 2*d*) agrees well with the predicted structure (electronic supplementary material, figure S2), consistent with the strength and robustness of the molecular replacement calculations.

Both the structure and the AF2 prediction show that the 'loop' is in fact an α-helical 'switchback', in which the helix entering the loop from the N-terminal side continues beyond its pairing with Nuf2, reverses direction into a segment with a partly disordered loop (using 'loop' in the stricter sense) as it turns back into an α helix, which continues into the region paired again with Nuf2. The Nuf2 chain is a continuous helix opposite the entire switchback. The short, disordered segment in the human Ndc80 structure corresponds (in the predictions) to the segment of *Saccharomyces cerevisiae* Ndc80 containing the substitutions in a seven-alanine mutant shown to fail in the transition to end-on attachment in budding yeast [27] (figure 2*a*). The very close correspondence of predicted and experimental loop structures for human Ndc80 : Nuf2 give us confidence in the predictions for other species, including the budding yeasts. The success of predictions for the head-shaft transition and its interaction with Dam1 described below also supports the credibility of the AF2 models.

2.2. Interaction of the DASH/Dam1c subunit Dam1 with the Ndc80c

Genetic, biochemical and cross-linking data suggest that a segment of the extended C terminus of the Dam1 subunit binds with a region of Ndc80 : Nuf2 near the position at which the Ndc80 and Nuf2 polypeptide chains transition from their paired, CH domains into a helical coiled-coil [1,17,19]. Various trial calculations in multi-chain AF2, in which we varied the details of the Dam1 segment we included, led to a self-consistent prediction for binding, in which two stretches of conserved Dam1 residues (252–270 and 290–305) (figure 3*a*; electronic supplementary material, data S5) showed the highest confidence scores. The predicted structure of the docked segment

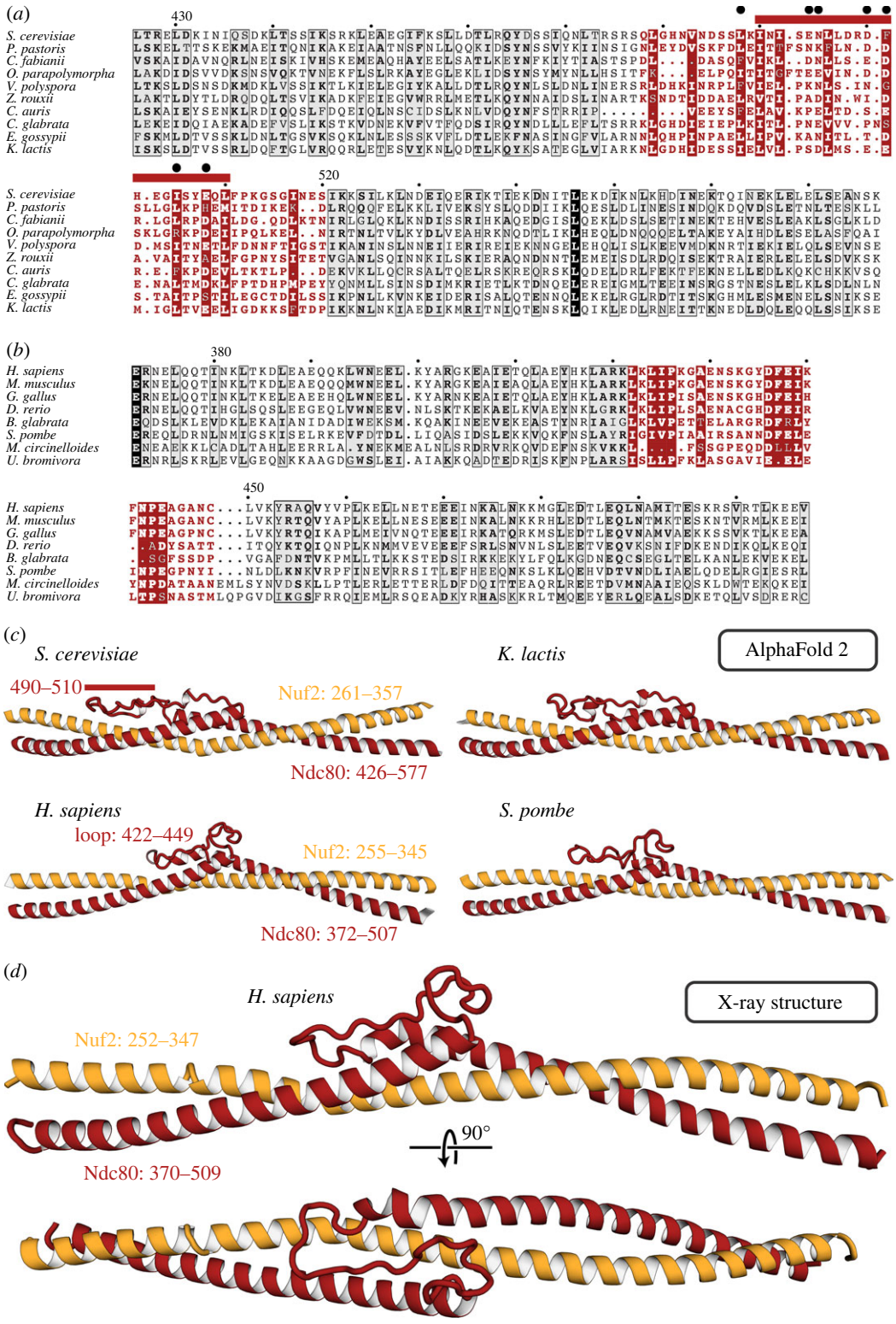

Figure 2. The Ndc80 loop. (*a*) Sequence alignment for the Ndc80 loop and adjacent residues for budding yeasts. Numbers above the sequences are for *S. cerevisiae*, residues 426–577. The loop residues are in red. The red bar above the alignment corresponds to the longest segment that can be deleted without lethality [27]. The black dots are residues mutated to alanine in the temperature-sensitive mutant *ndc80-7A* [27]. (*b*) Sequence alignment for the Ndc80 loop and adjacent residues for metazoans plus non-budding fungi. Numbers correspond to *H. sapiens*, residues 372–507. The loop residues are in red. (*c*) AF2 predictions of Ndc80 loop structures for two budding yeasts, human and fission yeast. The extended loop that doubles back between the two overlapped helices at either end is substantially longer in budding yeast, with the structural difference coinciding almost precisely with the longest non-lethal deletion (red bar, residues 490–510). For illustrations of the predictions with AF2 confidence levels, see electronic supplementary material, figure S2*a*. (*d*) Cartoon representation of the crystal structure of the human loop segment of Ndc80 : Nuf2. The view of the upper cartoon is the same as the view of the prediction for the human structure in (*c*). A full comparison is in the electronic supplementary material, figure S2.

suggested that a fusion construct of part of the Dam1 C terminus (residues 252–305) with the Nuf2 N terminus, combined with a deletion of residues between the two conserved stretches (residues 271–289), might ensure high local concentration and increase the likelihood of obtaining informative crystals. We therefore made the inferred Ndc80 : Dam1-Nuf2

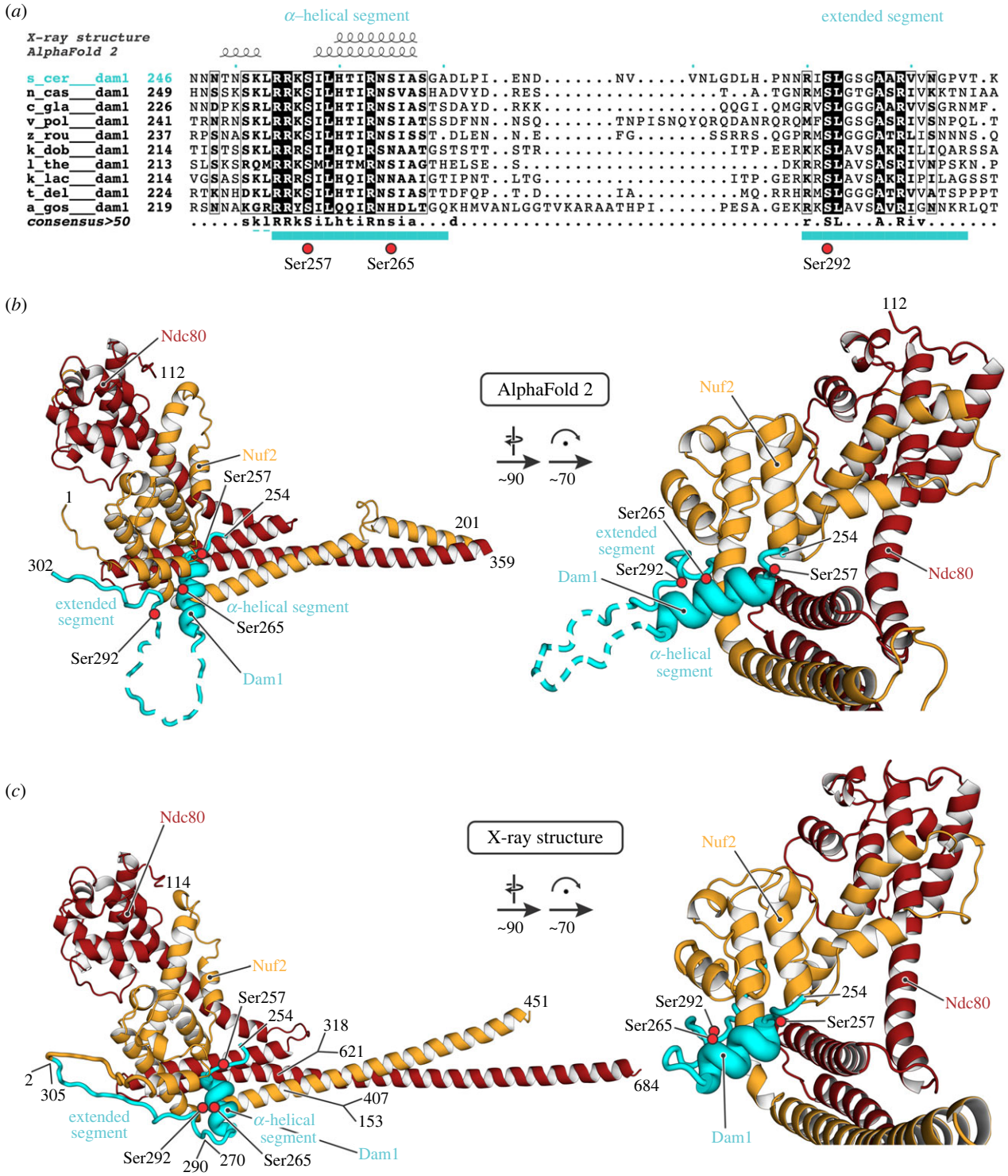

Figure 3. Association of a yeast Dam1 segment with the globular 'head' of Ndc80 : Nuf2. (*a*) Sequence alignment for budding yeasts, showing the Dam1 region of *S. cerevisiae* residues 246–307 (the full alignment is shown in electronic supplementary material, data S3). Cyan bars below the sequences are residues of the conserved α-helical and extended segments, respectively, that were modelled in the crystal structure here. Dashed lines are residues that were included in the construct but not modelled. Serine residues 257, 265 and 292, which can be phosphorylated by Ipl1, are indicated by red circles. (*b*) AF2 prediction for the residues shown. The dashed loop in Dam1 had very low reported confidence values and predicted variably from run to run. (*c*) Cartoon representation of the crystal structure of the Ndc80 : Dam1-Nuf2 fusion, residues as shown. The discontinuities in Ndc80 and Nuf2 are due to use of the Ndc80c 'dwarf' design to produce the construct [13]. The deletion of 19 residues in Dam1 corresponds to the low-confidence loop in (*b*). The 'prediction' for the globular domains is essentially precise, as the coordinates for the same sequences are in the PDB. Note that the position of the short Dam1 α helix is shifted by about 3 Å from its position in the prediction (electronic supplementary material, figure S4*c* and *e*). Red circles are the positions of serines 257, 265 and 290 (OG oxygen atoms). See also electronic supplementary material, figure S4.

fusion construct as part of the dwarf-Ndc80c, expressed and purified the recombinant protein, and obtained crystals in space group $P3_212$ ($a = b = 130.0$ Å, $c = 216.3$ Å). Molecular replacement with the Ndc80-Nuf2 component from PDB-ID 5TCS [13] and initial refinement without any Dam1 model yielded unbiased difference density for the Dam1 segment (electronic supplementary material, figure S3), allowing us to build and refine a model (data and refinement statistics in the

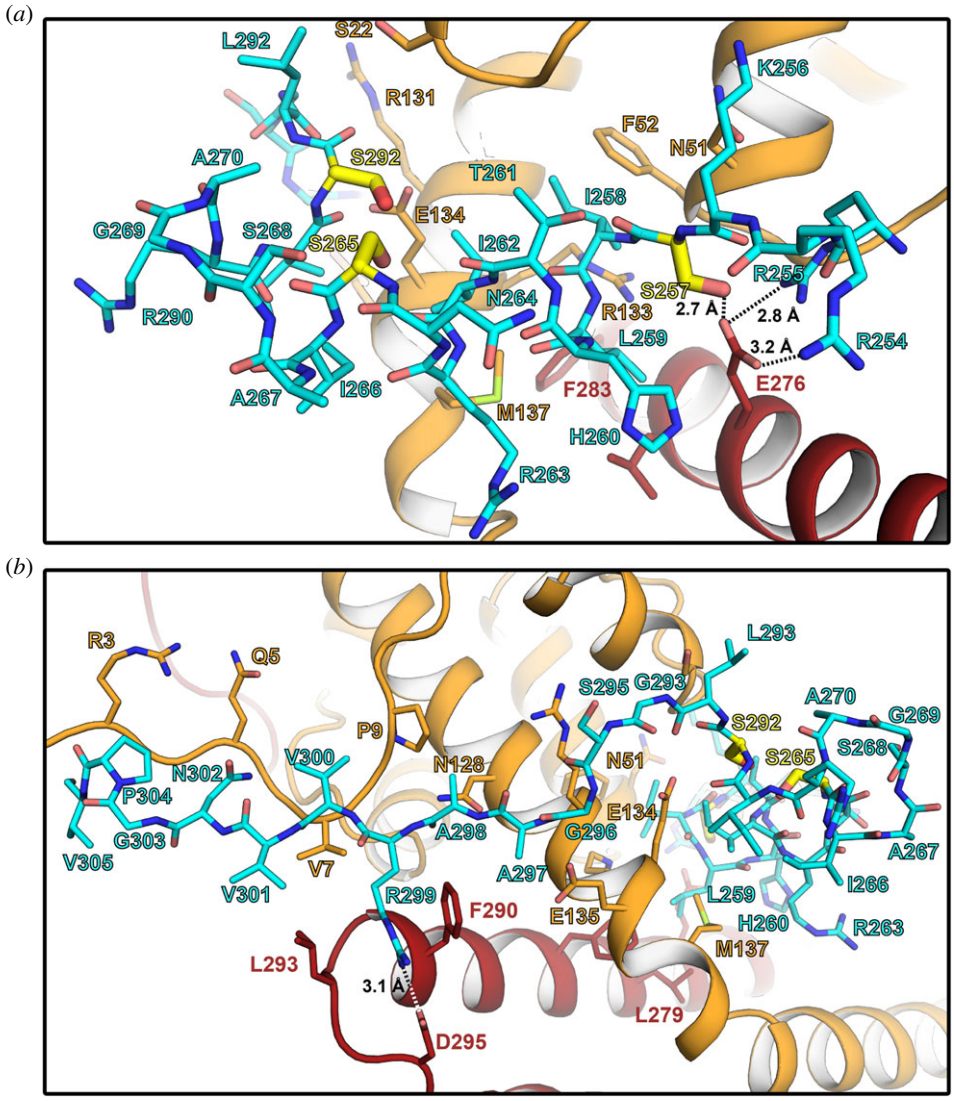

Figure 4. Close-up of the Dam1 : Ndc80c contacts. (*a*) Interactions between the Dam1 α-helical segment (cyan) and Ndc80 : Nuf2 (red and orange, respectively). Serine residues 257, 265 and 292 that are targets for phosphorylation by Ipl1/Aurora B are shown in yellow. The side chain of Ser257 is close to conserved Ndc80 glutamate 276 and its phosphorylation would result in electrostatic repulsion. (*b*) Interactions between the Dam1 extended segment (cyan) and Ndc80 : Nuf2 (red and orange, respectively). Note the salt bridge between conserved Dam1 residue Arg299 and Ndc80 Asp295.

electronic supplementary material, table S1). The Spc24-Scp25 component had dissociated during crystallization, and only the Ndc80 : Dam1-Nuf2 heterodimer was present in the crystals. The model and a comparison with the AF2 prediction are in figure 3*b*,*c*. The regions of the prediction with good confidence scores correspond well to the experimental result (electronic supplementary material, figure S4). A small difference in the short α helix (residues 258–267) does not substantially reorganize any of the side chain interactions.

Dam1 binds Ndc80 : Nuf2 with an α-helical segment, which rests in a cleft between the coiled-coil and the globular head domains, and an extended segment, which runs along the N terminus of Nuf2, but also contacts Ndc80 (figure 3*b* and *c*). The residues connecting the two segments, which are not conserved (figure 3*a*), are predicted to be flexible by AF2; we omitted them in the construct we crystallized. Molecular details of the interactions are shown in figure 4. A salt bridge between Dam1 Arg299 and Ndc80 Asp295, both conserved across budding yeasts (electronic supplementary material, data S3 and S5), anchors the C-terminal extended segment of the Dam1 fragment (figure 4*b*). The Dam1 sequence in the structure also includes three serines (residues 257, 265 and 292) (figure 3*a*), the first and third conserved among budding yeasts and the second largely so, that are potential Ipl1 targets for regulating Ndc80c binding (electronic supplementary material, data S5) [20]. The structure suggests that phosphorylation of serines 257 and 265 would substantially weaken the contact (figure 4*a*). Ser257 is opposite conserved Glu276 of Ndc80 and its phosphorylation would lead to electrostatic repulsion; serine 292 is well exposed in the model, but the thermal parameter in that segment of polypeptide chain is relatively high (electronic supplementary material, figure S4*b*), and electrostatic repulsion of a phosphoserine side chain by nearby negative charge might in principle weaken the contact and make phosphorylation of the other two sites more likely.

2.3. Location of a flexible hinge in Ndc80c

Electron micrographs of intact, recombinant Ndc80c suggest the presence of a variable bend in the shaft between the Ndc80 : Nuf2 globular domains and the four-way junction with Spc24 : Spc25 [3,34]. Although the bend was initially proposed to coincide with the position of the loop, which was an

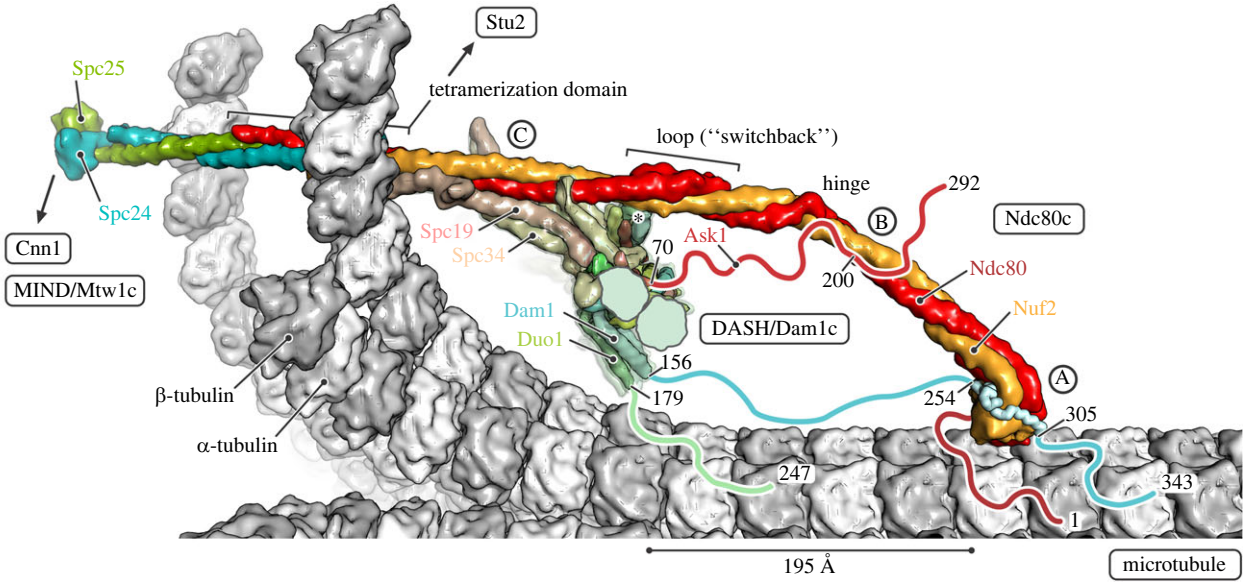

Figure 5. Model of the interactions of yeast Ndc80c with DASH/Dam1c and a kinetochore microtubule (MT). In the close-up view, a single Ndc80c in 'end-on' attachment to a curled MT is shown. α- and β-tubulin subunits are coloured white and grey, respectively. Ndc80c subunits are coloured as in figure 1. The DASH/Dam1c ring, composed of 17 heterodecameric complexes, is partially cut for illustration. Flexible extensions for which interactions with their binding partner are not yet structurally characterized were omitted from the models and drawn schematically as lines, including the N terminus of Ndc80 (red) and the C termini of Ask1 (red), Dam1 (cyan) and Duo1 (green). The N termini of Dam1 and Duo1 are not shown; an asterisk indicates their location next to the Ndc80c loop. Relevant residues are numbered. The three interactions between Ndc80c and DASH/Dam1c are labelled A, B and C [1,16]. Interaction A is defined by binding of the C-terminal Dam1 extension to the Ndc80 : Nuf2 head domains. The segment observed in the crystal structure here is shown in ribbon representation. Interaction B is between the C terminus of Ask1 and the Ndc80 : Nuf2 coiled-coil between the head and the hinge. Interaction C involves binding of the Spc19 : Spc34 protrusion domain to the Ndc80 : Nuf2 coiled-coil between the loop and tetramerization domains. See Material and Methods for details of how the model was obtained.

evident discontinuity in the alignment of predicted Ndc80 and Nuf2 coiled-coil sequences, measurements of its average position in published electron micrographs suggested a location between the globular domains and the loop [35], probably coincident with preferential proteolytic cleavage points, detected in our early work on the yeast Ndc80c, C-terminal to Ndc80 lysines 380 and 409 (electronic supplementary material, data S3) and Nuf2 lysines 220 and leucine 237 (electronic supplementary material, data S4) [2]. AF2 predictions for Ndc80 : Nuf2 across this region show a bend at Ndc80 residue 412 and Nuf2 residue 245, with some variation in the bend angle and direction depending on the length of the Ndc80 : Nuf2 segment submitted for prediction. One of the cleavages is consistent with the predicted hinge position, a likely point of proteolytic sensitivity; the other is consistent with some instability of the exposed C terminus of the coiled-coil, allowing the protease(s) to cleave somewhat further toward the globular head. The position of the predicted hinge is also consistent with the observed, variable kink in electron micrographs [4]. Figure 5 incorporates this predicted hinge into an overall composite model of full-length Ndc80c.

3. Discussion

The two structures reported here are both examples of using AF2 predictions to generate hypotheses for constructs likely to yield informative structures. For example, to design the particular loop construct that yielded the structure shown in figure 2*d*, ambiguities of coiled-coil heptad matching would have required a series of alternative pairings of the two chains on both sides of the loop itself, and the pairing C-terminal to the Ndc80 switchback is in fact half a heptad shifted from the best guess we had made previously, extrapolating from the structure of the four-way junction. AF2 predictions of the intervening coiled-coil region suggest how shifts in register (from the simple heptad-matched prediction) restore the experimentally determined pairing at the connection with Spc24 : Spc25 [13]. The Dam1 segment docking would have been even harder to guess, as the successful design involved noticing a likely covalent linkage with Nuf2 (to ensure that the Dam1 fragment would be present in a crystal) and a deletion between the two ordered segments of Dam1. The structure also illustrates a modest limitation of the prediction, in the details of contacts between the short Dam1 *α* helix and the Ndc80 : Nuf2 head (electronic supplementary material, figure S4*c*).

The consistency of both the structure predictions and the final structures with genetic and biochemical data in the literature, as well as with each other, adds confidence to those predictions for which we do not yet have direct structural confirmation. For example, as illustrated in figure 2, the longest segment that could be deleted without lethality, in published experiments on the role of the loop in the transition to end-on microtubule attachment [27], coincides precisely with the region in Ndc80 of budding yeasts (*S. cerevisiae* and *K. lactis*, in figure 2) that appears in alignments as an 'insertion' into Ndc80 loops of metazoans and even of fission yeast (see electronic supplementary material, data S1, Ndc80 sequence for *S. cerevisiae* starting at residue 490). Similarly, the AF2 predictions place Dam1 residues phosphorylated by Ipl1 at interface positions consistent with the physiological consequences of their modification.

We have integrated the information from the structures reported here with previously described analyses [16,35] to generate the composite picture in figure 5. In addition to the switchback structure of the loop and the structurally defined interaction of the Dam1 segment with the Ndc80 : Nuf2

globular domain, we have included additional contacts, based on inferences from biochemical and cross-linking mass spectrometry data in the literature [1], conservation of segments in the flexible extensions of DASH/Dam1c components (electronic supplementary material, data S5 and S6), and sites at which phosphorylation affects microtubule attachment or detachment. In addition to interactions with DASH/Dam1c contacts, the regions of Ndc80c in the model in figure 5 that rely on AF2 predictions rather than on experimentally determined structures are consistent with published cross-linking mass spectrometry results for Ndc80c from *S. cerevisiae* [36] and human [12] (electronic supplementary material, figure S5) and with direct correlation analysis based on sequences from over 1000 fungal species [35].

DASH/Dam1c binding at end-on attached kinetochores relies on oligomerization into rings, interactions with the microtubule lattice, and direct contacts with several Ndc80 complexes that by themselves bind microtubules. The removal (by proteolysis with elastase) of the C-terminal 'tails' of Dam1, Duo1 and Ask1 disables microtubule association of DASH/Dam1c heterodecamers *in vitro* as well as its polymerization into microtubule-encircling rings [37]. Additional experiments indicate that the tails of Dam1 and Duo1, but not of Ask1, are the principal microtubule contacts [15,38]. The negatively charged, flexible, C-terminal extensions of tubulin subunits are not required for DASH/Dam1c ring formation [37]. We therefore do not expect the microtubule contacts to be merely electrostatic compensation by positively charged residues but instead specific site-binding on the microtubule surface.

For Dam1, two short stretches of residues conserved among budding yeast are plausible candidates for the presumed microtubule contacts (electronic supplementary material, data S5). One is at the C terminus of the Dam1 polypeptide chain (approximate residue range from 335 to 343); the other is in the middle of the extended segment between the structured, α-helical bundle at the core of the heterodecamer and the segment that binds the Ndc80 : Nuf2 globular head (approximate residue range from 210 to 226). The latter includes conserved Mps1 phosphorylation sites serines 218 and 221, which appear to promote end-on attachment [39]. When the Ndc80 : Nuf2 head is bound to a kinetochore microtubule, with a docked Dam1 segment, both candidate contacts will be close to the microtubule surface (figure 5). Duo1 and Dam1 emerge from the helical bundle of a DASH/Dam1c heterodecamer as a predicted, flexibly attached, approximately 30-residue, α-helical coiled-coil (Dam1 residues 121–156, Duo1 residues 152–179, both segments moderately well conserved among budding yeast; electronic supplementary material, data S5 and S6), allowing Duo1 residues 180 to 247 to project toward the microtubule. Conserved residues near the Duo1 C terminus (electronic supplementary material, data S6) are therefore also candidate microtubule contacts.

Deletion of most of the Dam1 C-terminal extension (temperature-sensitive mutant Dam1–19, which has a stop codon at position 205) causes slow growth at permissive temperatures and collapsed spindles at the restrictive temperature [15,40]. The mutant lacks both the potential microtubule interactions described above and the Ndc80c contact analysed here, but the potential Duo1 microtubule interactions remain, as do the Ask1 and Spc19:Spc24 contacts with Ndc80c. These compensating interactions probably explain why the deletion is lethal only at 37°C. A similar interdependence may also account for the *in vitro* consequences of serine to aspartate mutations at positions 257, 265 and 292 [41]. Indeed, we should expect redundancy to characterize kinetochore assembly, in view of its critical role in assuring faithful segregation of genetic information during cell division.

Interactions of DASH/Dam1c with Ndc80, defined by mass spectrometry cross-linking [1], include not only the segments of Dam1 included in the crystal structure in figure 3 (interaction A) but also segments in the C-terminal extensions of Ask1 (interaction B) and of the Spc19 : Spc34 heterodimer that forms the protrusion domain of the DASH/Dam1c (interaction C). The cross-linked Ask1 segment centres on Ser200; phosphorylation of this residue by Ipl1 promotes dissociation [19]. Cdc28/Cdk1 phosphorylation of Ask1 at serine 250, just at the edge of the cross-linked region, promotes DASH/Dam1c assembly on microtubules [42–44]. C-terminal parts of Spc19 : Spc34 together form the prominent protrusion that projects from the helical bundle at the core of the DASH/Dam1c heterodecamer. As suggested in figure 5, the protrusion is in a position to associate closely with the Ndc80 : Nuf2 shaft between the loop and the tetramerization four-way junction. Cross-links between residues in Spc34 and Ndc80 detected by mass spectrometry span the entire extent of the Spc19 : Spc34 protrusion, centred on the Ipl1 phosphorylation site at Thr199 [1].

The Ndc80 loop participates in contacts essential for the transition from lateral to end-on kinetochore–microtubule attachment, in both yeast and human cells [27,45]. The six alanine substitutions in budding yeast Ndc80 that disrupt this transition [27] precisely span the disordered segment in the loop (figure 2). Because that segment is not essential for the structural integrity of Ndc80c, we infer that it probably binds some other kinetochore component or regulatory element. Although DASH/Dam1c is also essential for the end-on transition [27], the loop is not among the three contacts with Ndc80 defined by the published cross-linking experiments, discussed above, that motivated parts of the model in figure 5. The N-terminal extensions of Dam1 and Duo1 (60 and 57 residues, respectively), including an Ipl1 phosphorylation site at Dam1 serine 20 [20], project together from the helical bundle of the heterodecamer relatively close to the loop (see asterisk in figure 5) and hence might be loop contacts.

In fission yeast, the properties of temperature-sensitive mutants in *S. pombe* Ndc80 suggest that the loop has a role in recruiting Dis1/TOG and Alp7/TACC-Alp14/TOG, orthologues of Stu2 [46,47]. In human cells, their orthologue, chTOG, also interacts with Hec1 (human Ndc80), at a yet-to-be-identified site, and like Stu2, has an Aurora-B independent role in microtubule-attachment error correction [48]. Although the C-terminal segment of Stu2 binds the Ndc80c tetramerization domain, not the loop [21], we cannot rule out additional functional contacts, either direct or indirect [49]. Recent work presents evidence that the loop directs local clustering of human Ndc80c *in vitro* and shows that in cells, loop deletion or targeted mutation extends the spindle assembly checkpoint and delays anaphase [33]. Human cells lack DASH/Dam1c, however, and recruit the non-homologous Ska complex instead [50], and their centromeres bind bundles of at least 10 microtubules [51,52], rather than just one, probably with higher Ndc80c density than in yeast cells [53]. The correspondence of predicted loop structures from metazoans and fission yeast, whose centromeres bind several microtubules, suggests that the loop might have a role in coordinating interaction

with multiple microtubules. Thus, despite similar functional outcomes, not all the molecular interactions in loop-directed, end-on binding need to be homologous in metazoans and budding yeast.

4. Material and methods

4.1. AF2 predictions

For the AF predictions, we ran AF2, implemented either by SBgrid (version 2.1.1) or the O2 cluster at Harvard Medical School (version 2.2.2).

4.2. Ndc80c loop X-ray structure determination

To express the loop region of human or yeast Ndc80c, as a recombinant heterodimer, we cloned codon-optimized synthetic genes (IDT) coding for Ndc80 (residues 370–509 for human Ndc80, electronic supplementary material, data S1) with a TEV protease-cleavable 6-His tag and Nuf2 (residues 252–347 for human Ndc80; electronic supplementary material, data S2) into the respective multiple cloning sites of pETDuet-1. To facilitate formation of the Ndc80-Nuf2 heterodimer, we introduced four cysteine residues, two on the respective N and C termini of Ndc80, and another two on those of Nuf2. Proteins were co-expressed in Shuffle T7 *E. coli* (New England Biolabs). Low yield of the expressed yeast protein led us to focus on the human complex. We grew a total of 6 l of culture in 12 2 l baffled flasks at 37°C with shaking at 225 rpm to an O.D. of 0.8. Cells were then induced with 200 µM IPTG and incubated overnight at 18°C with shaking at 225 rpm. Cells were harvested by centrifugation and resuspended in 150 ml of a buffer containing 50 mM TRIS pH 8.0, 250 mM NaCl, 10 mM imidazole pH 8.0, 5 mM β-mercaptoethanol, 1 mM PMSF, 1 µg ml^{-1} pepstatin, 1 µg ml^{-1} aprotinin, 1 µg ml^{-1} leupeptin, 83 µg ml^{-1} lysozyme and 30 µg ml^{-1} DNase I. Cells were lysed by sonication, and the lysate was clarified by centrifugation and applied to Ni-NTA agarose equilibrated with buffer containing 20 mM TRIS pH 8.0, 100 mM NaCl, 10 mM imidazole pH 8.0 and 5 mM β-mercaptoethanol (equilibration buffer). Bound material was washed with equilibration buffer containing 20 mM imidazole pH 8.0 and 500 mM NaCl and then with equilibration buffer. Proteins were eluted with equilibration buffer containing 400 mM imidazole pH 8.0 and 50 mM NaCl. Eluates were treated overnight with TEV protease to remove the 6-His tag from the N terminus of Ndc80 and subjected to anion exchange chromatography using a HiTrap Q HP column (Cytiva), followed by size-exclusion chromatography using a HiLoad Superdex 200 26/60 column (Cytiva) equilibrated with 10 mM HEPES pH 7.5, 100 mM NaCl and 50 mM β-mercaptoethanol.

The human Ndc80c loop complex was concentrated to 25 mg ml^{-1} in an Amicon centrifugal concentrator in a buffer containing 10 mM HEPES pH 7.5, 100 mM NaCl, 2 mM tris(2-carboxyethyl)phosphine (TCEP) and 50 mM β-mercaptoethanol. The protein complex was crystallized by hanging drop vapour diffusion using 1 µl protein solution and 1 µl of a well solution containing 20% (w/v) polyethylene glycol 4000, 0.1 M TRIS pH 8.6 and 0.2 M magnesium chloride. Crystals were cryo-protected by a 3–5 min soak in well solution supplemented with 25% (v/v) glycerol and flash-frozen in liquid nitrogen.

The complex crystallized in space group C_2 ($a = 49.9$ Å, $b = 72.3$ Å, $c = 80.1$ Å). Data to a minimum Bragg spacing of 1.9 Å were recorded on the NE-CAT beamline 24-ID-C at the Advanced Photon Source (APS), and indexed, integrated, scaled and merged using the DIALS-AIMLESS pipeline in xia2 [54] (electronic supplementary material, table S1). The structure was determined by molecular replacement using Phaser [55] as implemented in CCP4 Cloud [56]. Search models consisted of four fragments of the AF2-generated structure. Model building was carried out in Coot [57], and refinement, in Phenix [58]. We used MolProbity [59] for structure validation. The final model includes the following residues (electronic supplementary material, table S2, and data S1 and S2): $Ndc80^{370–509}$, $Nuf2^{252–347}$, plus a cysteine residue at each end of each chain and one serine (left after proteolysis by TEV) at the N terminus of Ndc80. Model statistics are shown in the electronic supplementary material, table S1.

4.3. Ndc80 : Dam1-Nuf2 X-ray structure determination

We designed an Ndc80 : Dam1-Nuf2 fusion construct, with sequences from *S. cerevisiae*, based on the AF prediction, as described in the main text. To express this construct as recombinant protein, we modified a previously constructed pETDuet vector coding for truncated (dwarf) versions of Ndc80 and Nuf2 [13,21], by fusing segments from the C-terminal extension of Dam1 (residues 252–270 and 290–305) to the N terminus of Nuf2 (electronic supplementary material, data S3–S5). To express a Dam1-fused heterodimer, we co-transformed Rosetta2(DE3)pLysS with the modified construct and a pRSFDuet plasmid containing the genes for truncated dwarf versions of Spc24 and Spc25 [13,21]. We grew a total of 6 l of culture in 12 2 l baffled flasks at 37°C with shaking at 225 rpm to an O.D. of 0.8. Cells were then induced with 200 µM IPTG, followed by overnight incubation at 18°C with shaking at 225 rpm. The Dam1-fused, dwarf-Ndc80c was purified as described above for the recombinant loop region of human Ndc80c (see above), except that the buffer of the final gel filtration step contained 2 mM TCEP instead of β-mercaptoethanol.

The dwarf-Ndc80c with the Dam1 segment fused to the N terminus of Nuf2 was concentrated to 15 mg ml^{-1} in an Amicon centrifugal concentrator in a buffer containing 10 mM HEPES pH 7.5, 100 mM NaCl and 2 mM TCEP. The protein complex was crystallized by hanging drop vapour diffusion using 1 µl protein solution and 1 µl of a well solution containing 12% (v/v) 2-methyl-2,4-pentanediol (MPD) and 0.1 M ADA buffer pH 6.8. Crystals were cryo-protected by soaking for 3–5 min in well solution containing 25% (v/v) MPD followed by flash-freezing in liquid nitrogen.

Diffraction data from multiple crystals were recorded on the NE-CAT beamline 24-ID-E at the APS, each with a total range of 360°. Data were indexed, integrated, scaled and merged using the DIALS-aimless pipeline [54,60] as implemented in xia2 [54]. To achieve higher redundancy and thus get better estimates of the intensities of weak reflections, nine isomorphous datasets were scaled together and merged. Indexing of the diffraction pattern showed a primitive hexagonal Bravais lattice for the crystallized complex. Scaling and molecular replacement (see below) showed that the space group was $P3_212$ ($a = b = 130.0$ Å, $c = 216.3$ Å) (electronic supplementary material, table S1).

The structure was determined by molecular replacement using Phaser [55] as implemented in Phenix [58]. The search model consisted of the Ndc80 and Nuf2 heads with a stretch of coiled-coil. We could not place any search models that contained Spc24 : Spc25, nor did we observe any density for Spc24: Spc25 in difference maps. From the placement of Ndc80 : Nuf2 it was evident that the crystal packing did not allow the presence of Spc24 : Spc25 as seen in the dwarf-Ndc80c structure [13,21]. Thus, during crystallization, Spc24 : Spc25 had dissociated from Ndc80 : Dam1-Nuf2, and there were two copies of a Ndc80 : Dam1-Nuf2 complex in the asymmetric unit.

To obtain structure factors for model building, phase improvement and structure refinement, we submitted unmerged data after integration with xia2 [54] to the STARANISO server [61]. After excluding frames with high-merging R values, we used the 'unmerged data' protocol for Bayesian estimation of structure amplitudes. We kept the default value of 1.20 for the local mean $I/\sigma(I)$ as diffraction cut-off criterion, which resulted in diffraction limits at the principal axes of the ellipsoid fitted to the diffraction cut-off surface of 3.71 Å (principal axis 0.894 **a*** - 0.447 **b***), 3.71 Å (principal axis **b***) and 3.14 Å (principal axis **c***). Final merging statistics from the STARANISO processing are given in the electronic supplementary material, table S1. We used uniquify from CCP4 [60] to select 5% of the reflections for the calculation of free R factors and B-sharpened the observed amplitudes with phenix.remove_aniso (b_iso = 80.0).

To obtain the best possible, unbiased electron density for the Dam1 segment, we modelled and refined Ndc80 : Nuf2 to convergence before modelling the Dam1 segment. For this modelling, we manually adjusted the Ndc80 and Nuf2 models in O [62] and Coot [57], followed by refinement with phenix.refine [58], and density modification with RESOLVE [58]. We ran RESOLVE with twofold non-crystallographic symmetry (NCS) averaging, restricted to regions occupied by Ndc80 and Nuf2. We defined five NCS groups (Ndc80: residues 114–237, 238–626, 627–684; Nuf2: residues 13–136, 137–451) and calculated transformation matrices and masks based on the corresponding structures. Because the density corresponding to the Dam1 segment differed substantially between the two NCS copies (see below), this region was excluded from NCS averaging. We also outlined the Dam1 segment density by placing dummy atoms, which we then used to exclude this region from the solvent mask in RESOLVE. We input a solvent content fraction of 0.72. We also calculated feature-enhanced maps with phenix.fem [63]. An electron density map from the last iteration of model building, refinement and phase improvement before modelling the Dam1 segment and a final map are shown in the electronic supplementary material, figure S3.

We observed that density for the Dam1 segment fused to the second copy of the Ndc80 : Nuf2 head in the asymmetric unit was much weaker than the first, and its appearance was of insufficient clarity to build a molecular model. Superposition of our Ndc80:Dam-Nuf2 structure from NCS position 1 onto Ndc80 : Nuf2 of NCS position 2 showed that a Dam1 segment bound as observed at position 1 would clash at position 2 with its crystallographic symmetry mate. Thus, the crystal packing prevented uniform ordering of the Dam1 segment at position 2.

We refined final structure with phenix.refine [58] against B-sharpened structure amplitudes obtained from STARANISO. The final model includes the following residues (electronic supplementary material, table S2 and electronic supplementary material, data S3–S5): Ndc80$^{114–318,\ 621–684}$ (chain A), Nuf2$^{2–153,\ 407–451}$ (chain B), Dam1$^{254–270,\ 290–305}$ (chain B), Ndc80$^{115–318,\ 621–684}$ (chain C) and Nuf2$^{9–153,\ 407–451}$ (chain D). In addition to standard stereochemical restraints, we used secondary structure, Ramachandran and torsion angle NCS restraints. Target function weight optimization was turned on. For grouped anisotropic B factor refinement, TLS groups were obtained from the TLS Motion Determination (TLSMD) web server [64] (electronic supplementary material, table S2). We used MolProbity [59] for structure validation. The final model statistics are shown in the electronic supplementary material, table S1.

4.4. Model of the yeast kinetochore–microtubule interface

We modelled a 13-protofilament MT based on the cryoEM structure of a yeast tubulin dimer polymerized with GTP *in vitro* (PDB-ID 5W3F) [65]. As published, we used lattice parameters for the MT tube with a helical rise of 83.3 Å and a rotation of 0.43° between dimers within a protofilament, and a helical rise of 9.65 Å and a rotation of −27.6° between protofilaments. The majority of kinetochore MTs in tomograms recorded from budding yeast were observed in in 'ram's horn' geometry [66], and we modelled the flaring of protofilaments at the MT plus end by matching the average curvature of the tomograms with the curvature observed in various structures of bent tubulin protofilaments (PDB-IDs 3J6H, 3RYH, 4HNA, 4FFB, 6MZG).

To model a MT-bound yeast Ndc80c, we first docked the AF2 prediction of Ndc80 : Nuf2 up to a few residues beyond the hinge (Ndc80$^{115–444}$, Nuf2$^{1–277}$) onto the MT. For this, we used the structure of the human Ndc80 : Nuf2 head domain bound to the MT lattice (PDB-ID 3iZ0) [7] for superposition of tubulin and the Ndc80 head domain (*H. sapiens* residues 110–202). Next, we placed a composite model of two AF2 predictions, comprising sequence from Ndc80 : Nuf2 just before the hinge all the way to the Spc24 : Spc25 head domains (Ndc80$^{413–691}$, Nuf2$^{252–451}$, Spc25$^{1–89}$, Spc25$^{1–83}$; and Ndc80$^{619–691}$, Nuf2$^{404–451}$, Spc24$^{1–213}$, Spc25$^{1–221}$) with a hinge angle such that the coiled-coils of Ndc80 : Nuf2 (after the hinge) and Spc24 : Spc25 were approximately parallel to the microtubule axis. Finally, we re-modelled the hinge residues in plausible conformation using RosettaRemodel [67].

For the DASH/Dam1c, we manually placed one heterodecamer of the *S. cerevisiae* full-length AF2 prediction, including only the well-structured regions of the core complex with high confidence scores (Ask1$^{2–69}$, Dad1$^{14–73}$, Dad2$^{2–85,\ 116–133}$, Dad3$^{6–94}$, Dad4$^{2–72}$, Dam1$^{54–162}$, Duo1$^{61–180}$, Hsk3$^{2–69}$, Spc19$^{2–106}$, Spc34$^{2–118,157–264}$), into the cryoEM map of a DASH/Dam1c ring assembled around a MT [68] (note that the deposited map, EMD-5254, has the wrong hand and needs to be inverted), followed by rigid-body fitting with phenix.real_space_refine [69]. The full-length complex was then placed on the fitted core complex and 17-fold rotationally expanded around the MT axis. The whole DASH/Dam1c ring was then rotated around and translated along the MT axis such that interaction C [1,19] between the protrusion domain of one DASH/Dam1c heterodecamer and the MT-bound Ndc80c could be established. This juxtaposed Thr199 of Spc34, the residue that is phosphorylated by Ipl1 and regulates interaction C [19], and residue 583 of Ndc80, the position

of a five amino acid mutation (insertion) that abrogates interaction C [1]. It also allows for establishment of the interaction between Spc19 residues 128–165 and Nuf2 residues 399–429 [70]. The C termini of Spc19 and Sp34 form a coiled-coil at the tip of the DASH/Dam1c protrusion domain, which was not observed in the cryoEM reconstruction of the *C. thermophilum* DASH/Dam1c complex (because of its flexible attachment) but was inferred from sequence analysis [16]; AF2 also predicts it now. We used HADDOCK 2.4 [71] to dock the C-terminal Spc19 : Spc34 coiled-coil onto Ndc80 : Nuf2 and re-modelled the residues that connect it to the protrusion domain with RosettaRemodel [67]. The model of the DASH/Dam1c ring shown in figure 5 contains the following residues for each subunit: Ask1$^{1–70}$, Dad1$^{15–77}$, Dad2$^{1–73,\ 119–133}$, Dad3$^{6–35,\ 49–94}$, Dad4$^{3–70}$, Dam1$^{53–156}$, Duo1$^{58–179}$, Hsk3$^{3–66}$, Spc19$^{1–165}$, Spc34$^{1–295}$. We added the C-terminal Dam1 segment (residues 254–270, 290–305) from the crystal structure determined here by superposition of the Ndc80 head domains.

Data accessibility. The structure factors and refined atomic coordinates from the crystal structures determined in this study have been deposited in the Protein Data Bank under accession codes PDB-ID 8G0P (Ndc80c loop) and PDB-ID 8G0Q (Ndc80:Dam1-Nuf2).

Other data are provided in the electronic supplementary material [72].

Authors' contributions. J.A.Z.: conceptualization, data curation, formal analysis, investigation, methodology, validation, visualization and writing—review and editing; S.J.: data curation, formal analysis, investigation, methodology, supervision, validation, visualization, writing—original draft and writing—review and editing; S.C.H.: conceptualization, funding acquisition, project administration, supervision, validation, writing—original draft and writing—review and editing.

All authors gave final approval for publication and agreed to be held accountable for the work performed therein.

Conflict of interest declaration. We declare we have no competing interests.

Funding. This research was supported by the Howard Hughes Medical Institute (S.C.H. Investigator's budget) and by Postdoctoral Fellowship PF-21-188-01-CCB to J.A.Z. from the American Cancer Society.

Acknowledgements. We thank the staff of the NE-CAT beamlines, in particular Jon Scheurman, for help in data collection. NE-CAT is supported by NIH grant P30 GM124165, using resources of the APS, operated by Argonne National Laboratory under Contract DE-AC02-06CH11357. Portions of this research were conducted on the O2 High Performance Compute Cluster, operated by the Research Computing Group at Harvard Medical School. S.C.H. is an Investigator in the Howard Hughes Medical Institute.

References

1. Kim JO, Zelter A, Umbreit NT, Bollozos A, Riffle M, Johnson R, MacCoss MJ, Asbury CL, Davis TN. 2017 The Ndc80 complex bridges two Dam1 complex rings. *Elife* **6**, e21069. (doi:10.7554/eLife.21069)
2. Wei RR, Sorger PK, Harrison SC. 2005 Molecular organization of the Ndc80 complex, an essential kinetochore component. *Proc. Natl Acad. Sci. USA* **102**, 5363–5367. (doi:10.1073/pnas.0501168102)
3. Wang HW, Long S, Ciferri C, Westermann S, Drubin D, Barnes G, Nogales E. 2008 Architecture and flexibility of the yeast Ndc80 kinetochore complex. *J. Mol. Biol.* **383**, 894–903. (doi:10.1016/j.jmb.2008.08.077)
4. Ciferri C *et al.* 2005 Architecture of the human ndc80-hec1 complex, a critical constituent of the outer kinetochore. *J. Biol. Chem.* **280**, 29 088–29 095. (doi:10.1074/jbc.M504070200)
5. Wei RR, Al-Bassam J, Harrison SC. 2007 The Ndc80/HEC1 complex is a contact point for kinetochore-microtubule attachment. *Nat. Struct. Mol. Biol.* **14**, 54–59. (doi:10.1038/nsmb1186)
6. Ciferri C *et al*. 2008 Implications for kinetochore-microtubule attachment from the structure of an engineered Ndc80 complex. *Cell* **133**, 427–439. (doi:10.1016/j.cell.2008.03.020)
7. Alushin GM, Ramey VH, Pasqualato S, Ball DA, Grigorieff N, Musacchio A, Nogales E. 2010 The Ndc80 kinetochore complex forms oligomeric arrays along microtubules. *Nature* **467**, 805–810. (doi:10.1038/nature09423)
8. Wei RR, Schnell JR, Larsen NA, Sorger PK, Chou JJ, Harrison SC. 2006 Structure of a central component of the yeast kinetochore: the Spc24p/Spc25p globular domain. *Structure* **14**, 1003–1009. (doi:10.1016/j.str.2006.04.007)
9. Nishino T, Rago F, Hori T, Tomii K, Cheeseman IM, Fukagawa T. 2013 CENP-T provides a structural platform for outer kinetochore assembly. *EMBO J.* **32**, 424–436. (doi:10.1038/emboj.2012.348)
10. Malvezzi F, Litos G, Schleiffer A, Heuck A, Mechtler K, Clausen T, Westermann S. 2013 A structural basis for kinetochore recruitment of the Ndc80 complex via two distinct centromere receptors. *EMBO J.* **32**, 409–423. (doi:10.1038/emboj.2012.356)
11. Dimitrova YN, Jenni S, Valverde R, Khin Y, Harrison SC. 2016 Structure of the MIND complex defines a regulatory focus for yeast kinetochore assembly. *Cell* **167**, 1014–1027. (doi:10.1016/j.cell.2016.10.011)
12. Maiolica A, Cittaro D, Borsotti D, Sennels L, Ciferri C, Tarricone C, Musacchio A, Rappsilber J. 2007 Structural analysis of multiprotein complexes by cross-linking, mass spectrometry, and database searching. *Mol. Cell. Proteomics* **6**, 2200–2211. (doi:10.1074/mcp.M700274-MCP200)
13. Valverde R, Ingram J, Harrison SC. 2016 Conserved tetramer junction in the kinetochore Ndc80 complex. *Cell Rep.* **17**, 1915–1922. (doi:10.1016/j.celrep.2016.10.065)
14. Miranda JJ, De Wulf P, Sorger PK, Harrison SC. 2005 The yeast DASH complex forms closed rings on microtubules. *Nat. Struct. Mol. Biol.* **12**, 138–143. (doi:10.1038/nsmb896)
15. Westermann S, Avila-Sakar A, Wang HW, Niederstrasser H, Wong J, Drubin DG, Nogales E, Barnes G. 2005 Formation of a dynamic kinetochore-microtubule interface through assembly of the Dam1 ring complex. *Mol. Cell.* **17**, 277–290. (doi:10.1016/j.molcel.2004.12.019)
16. Jenni S, Harrison SC. 2018 Structure of the DASH/Dam1 complex shows its role at the yeast kinetochore-microtubule interface. *Science* **360**, 552–558. (doi:10.1126/science.aar6436)
17. Lampert F, Mieck C, Alushin GM, Nogales E, Westermann S. 2013 Molecular requirements for the formation of a kinetochore-microtubule interface by Dam1 and Ndc80 complexes. *J. Cell Biol.* **200**, 21–30. (doi:10.1083/jcb.201210091)
18. Miller MP, Asbury CL, Biggins S. 2016 A TOG protein confers tension sensitivity to kinetochore-microtubule attachments. *Cell* **165**, 1428–1439. (doi:10.1016/j.cell.2016.04.030)
19. Flores RL, Peterson ZE, Zelter A, Riffle M, Asbury CL, Davis TN. 2022 Three interacting regions of the Ndc80 and Dam1 complexes support microtubule tip-coupling under load. *J. Cell Biol.* **221**, jcb.202107016. (doi:10.1083/jcb.202107016)
20. Cheeseman IM *et al*. 2002 Phospho-regulation of kinetochore-microtubule attachments by the Aurora kinase Ipl1p. *Cell* **111**, 163–172. (doi:10.1016/S0092-8674(02)00973-X)
21. Zahm JA, Stewart MG, Carrier JS, Harrison SC, Miller MP. 2021 Structural basis of Stu2 recruitment to yeast kinetochores. *Elife* **10**, e65389. (doi:10.7554/eLife.65389)
22. Tanaka K, Mukae N, Dewar H, van Breugel M, James EK, Prescott AR, Antony C, Tanaka TU. 2005 Molecular mechanisms of kinetochore capture by spindle microtubules. *Nature* **434**, 987–994. (doi:10.1038/nature03483)
23. Grishchuk EL, McIntosh JR. 2006 Microtubule depolymerization can drive poleward chromosome motion in fission yeast. *EMBO J.* **25**, 4888–4896. (doi:10.1038/sj.emboj.7601353)
24. Umbreit NT, Miller MP, Tien JF, Ortola JC, Gui L, Lee KK, Biggins S, Asbury CL, Davis TN. 2014

Kinetochores require oligomerization of Dam1 complex to maintain microtubule attachments against tension and promote biorientation. *Nat. Commun.* **5**, 4951. (doi:10.1038/ncomms5951)

25. Kitamura E, Tanaka K, Kitamura Y, Tanaka TU. 2007 Kinetochore microtubule interaction during S phase in *Saccharomyces cerevisiae*. *Genes Dev.* **21**, 3319–3330. (doi:10.1101/gad.449407)
26. Tanaka K, Kitamura E, Kitamura Y, Tanaka TU. 2007 Molecular mechanisms of microtubule-dependent kinetochore transport toward spindle poles. *J. Cell Biol.* **178**, 269–281. (doi:10.1083/jcb.200702141)
27. Maure JF, Komoto S, Oku Y, Mino A, Pasqualato S, Natsume K, Clayton L, Musacchio A, Tanaka TU. 2011 The Ndc80 loop region facilitates formation of kinetochore attachment to the dynamic microtubule plus end. *Curr. Biol.* **21**, 207–213. (doi:10.1016/j.cub.2010.12.050)
28. Jin F, Bokros M, Wang Y. 2017 The phosphorylation of a kinetochore protein Dam1 by Aurora B/Ipl1 kinase promotes chromosome bipolar attachment in yeast. *Sci. Rep.* **7**, 11880. (doi:10.1038/s41598-017-12329-z)
29. Keating P, Rachidi N, Tanaka TU, Stark MJ. 2009 Ipl1-dependent phosphorylation of Dam1 is reduced by tension applied on kinetochores. *J. Cell Sci.* **122**, 4375–4382. (doi:10.1242/jcs.055566)
30. Tien JF, Umbreit NT, Gestaut DR, Franck AD, Cooper J, Wordeman L, Gonen T, Asbury CL, Davis TN. 2010 Cooperation of the Dam1 and Ndc80 kinetochore complexes enhances microtubule coupling and is regulated by aurora B. *J. Cell Biol.* **189**, 713–723. (doi:10.1083/jcb.200910142)
31. Lampert F, Hornung P, Westermann S. 2010 The Dam1 complex confers microtubule plus end-tracking activity to the Ndc80 kinetochore complex. *J. Cell Biol.* **189**, 641–649. (doi:10.1083/jcb.200912021)
32. Jumper J *et al*. 2021 Highly accurate protein structure prediction with AlphaFold. *Nature* **596**, 583–589. (doi:10.1038/s41586-021-03819-2)
33. Polley S, Müschenborn H, Terbeck M, De Antoni A, Vetter IR, Dogterom M, Musacchio A, Volkov VA, Huis In 't Veld PJ. 2022 Stable kinetochore-microtubule attachment requires loop-dependent Ndc80-Ndc80 binding. *bioRxiv*. 2022.08.25.505310.
34. Huis In 't Veld PJ, Jeganathan S, Petrovic A, Singh P, John J, Krenn V, Weissmann F, Bange T, Musacchio A. 2016 Molecular basis of outer kinetochore assembly on CENP-T. *Elife* **5**, e21007. (doi:10.7554/eLife.21007)
35. Jenni S, Dimitrova YN, Valverde R, Hinshaw SM, Harrison SC. 2017 Molecular structures of yeast kinetochore subcomplexes and their roles in chromosome segregation. *Cold Spring Harb. Symp. Quant. Biol.* **82**, 83–89. (doi:10.1101/sqb.2017.82.033738)
36. Tien JF *et al*. 2014 Kinetochore biorientation in *Saccharomyces cerevisiae* requires a tightly folded conformation of the Ndc80 complex. *Genetics* **198**, 1483–1493. (doi:10.1534/genetics.114.167775)
37. Miranda JJ, King DS, Harrison SC. 2007 Protein arms in the kinetochore-microtubule interface of the yeast DASH complex. *Mol. Biol. Cell.* **18**, 2503–2510. (doi:10.1091/mbc.E07-02-0135)
38. Legal T, Zou J, Sochaj A, Rappsilber J, Welburn JP. 2016 Molecular architecture of the Dam1 complex-microtubule interaction. *Open Biol.* **6**, 150237. (doi:10.1098/rsob.150237)
39. Shimogawa MM *et al*. 2006 Mps1 phosphorylation of Dam1 couples kinetochores to microtubule plus ends at metaphase. *Curr. Biol.* **16**, 1489–1501. (doi:10.1016/j.cub.2006.06.063)
40. Cheeseman IM, Enquist-Newman M, Muller-Reichert T, Drubin DG, Barnes G. 2001 Mitotic spindle integrity and kinetochore function linked by the Duo1p/Dam1p complex. *J. Cell Biol.* **152**, 197–212. (doi:10.1083/jcb.152.1.197)
41. Sarangapani KK, Akiyoshi B, Duggan NM, Biggins S, Asbury CL. 2013 Phosphoregulation promotes release of kinetochores from dynamic microtubules via multiple mechanisms. *Proc. Natl Acad. Sci. USA* **110**, 7282–7287. (doi:10.1073/pnas.1220700110)
42. Higuchi T, Uhlmann F. 2005 Stabilization of microtubule dynamics at anaphase onset promotes chromosome segregation. *Nature* **433**, 171–176. (doi:10.1038/nature03240)
43. Li Y, Elledge SJ. 2003 The DASH complex component Ask1 is a cell cycle-regulated Cdk substrate in *Saccharomyces cerevisiae*. *Cell Cycle.* **2**, 143–148.
44. Gutierrez A, Kim JO, Umbreit NT, Asbury CL, Davis TN, Miller MP, Biggins S. 2020 Cdk1 phosphorylation of the Dam1 complex strengthens kinetochore-microtubule attachments. *Curr. Biol.* **30**, 4491–4499. (doi:10.1016/j.cub.2020.08.054)
45. Shrestha RL, Draviam VM. 2013 Lateral to end-on conversion of chromosome-microtubule attachment requires kinesins CENP-E and MCAK. *Curr. Biol.* **23**, 1514–1526. (doi:10.1016/j.cub.2013.06.040)
46. Hsu KS, Toda T. 2011 Ndc80 internal loop interacts with Dis1/TOG to ensure proper kinetochore-spindle attachment in fission yeast. *Curr. Biol.* **21**, 214–220. (doi:10.1016/j.cub.2010.12.048)
47. Tang NH, Takada H, Hsu KS, Toda T. 2013 The internal loop of fission yeast Ndc80 binds Alp7/TACC-Alp14/TOG and ensures proper chromosome attachment. *Mol. Biol. Cell.* **24**, 1122–1133. (doi:10.1091/mbc.E12-11-0817)
48. Herman JA, Miller MP, Biggins S. 2020 chTOG is a conserved mitotic error correction factor. *Elife* **9**, e61773. (doi:10.7554/eLife.61773)
49. Miller MP, Evans RK, Zelter A, Geyer EA, MacCoss MJ, Rice LM, Davis TN, Asbury CL, Biggins S. 2019 Kinetochore-associated Stu2 promotes chromosome biorientation in vivo. *PLoS Genet.* **15**, e1008423. (doi:10.1371/journal.pgen.1008423)
50. van Hooff JJE, Snel B, Kops G. 2017 Unique phylogenetic distributions of the Ska and Dam1 complexes support functional analogy and suggest multiple parallel displacements of Ska by Dam1. *Genome Biol. Evol.* **9**, 1295–1303. (doi:10.1093/gbe/evx088)
51. O'Toole E, Morphew M, McIntosh JR. 2020 Electron tomography reveals aspects of spindle structure important for mechanical stability at metaphase. *Mol. Biol. Cell.* **31**, 184–195. (doi:10.1091/mbc.E19-07-0405)
52. Kiewisz R, Fabig G, Conway W, Baum D, Needleman D, Muller-Reichert T. 2022 Three-dimensional structure of kinetochore-fibers in human mitotic spindles. *Elife* **11**, e75459. (doi:10.7554/eLife.75459)
53. Suzuki A, Badger BL, Salmon ED. 2015 A quantitative description of Ndc80 complex linkage to human kinetochores. *Nat. Commun.* **6**, 8161. (doi:10.1038/ncomms9161)
54. Gildea RJ *et al*. 2022 xia2.multiplex: a multi-crystal data-analysis pipeline. *Acta Crystallogr. D Struct. Biol.* **78**, 752–769. (doi:10.1107/S2059798322004399)
55. McCoy AJ, Grosse-Kunstleve RW, Adams PD, Winn MD, Storoni LC, Read RJ. 2007 Phaser crystallographic software. *J. Appl. Crystallogr.* **40**, 658–674. (doi:10.1107/S0021889807021206)
56. Krissinel E *et al*. 2022 CCP4 Cloud for structure determination and project management in macromolecular crystallography. *Acta Crystallogr. D Struct. Biol.* **78**, 1079–1089. (doi:10.1107/S2059798322007987)
57. Emsley P, Lohkamp B, Scott WG, Cowtan K. 2010 Features and development of Coot. *Acta Crystallogr. D Biol. Crystallogr.* **66**, 486–501. (doi:10.1107/S0907444910007493)
58. Adams PD *et al*. 2010 PHENIX: a comprehensive Python-based system for macromolecular structure solution. *Acta Crystallogr. D Biol. Crystallogr.* **66**, 213–221. (doi:10.1107/S0907444909052925)
59. Chen VB, Arendall 3rd WB, Headd JJ, Keedy DA, Immormino RM, Kapral GJ, Murray LW, Richardson JS, Richardson DC. 2010 MolProbity: all-atom structure validation for macromolecular crystallography. *Acta Crystallogr. D Biol. Crystallogr.* **66**, 12–21. (doi:10.1107/S0907444909042073)
60. Winn MD *et al*. 2011 Overview of the CCP4 suite and current developments. *Acta Crystallogr. D Biol. Crystallogr.* **67**, 235–242. (doi:10.1107/S0907444910045749)
61. Tickle IJ, Flensburg C, Keller P, Paciorek W, Sharff A, Smart O, Vonrhein C, Bricogne G. 2022 The STARANISO server. See https://staraniso.globalphasing.org.
62. Jones TA, Zou JY, Cowan SW, Kjeldgaard M. 1991 Improved methods for building protein models in electron density maps and the location of errors in these models. *Acta Crystallogr. A* **47**, 110–119. (doi:10.1107/S0108767390010224)
63. Afonine PV, Moriarty NW, Mustyakimov M, Sobolev OV, Terwilliger TC, Turk D, Urzhumtsev A, Adams PD. 2015 FEM: feature-enhanced map. *Acta Crystallogr. D Biol. Crystallogr.* **71**, 646–666. (doi:10.1107/S1399004714028132)
64. Painter J, Merritt EA. 2006 Optimal description of a protein structure in terms of multiple groups undergoing TLS motion. *Acta Crystallogr. D Biol. Crystallogr.* **62**, 439–450. (doi:10.1107/S0907444906005270)

65. Howes SC, Geyer EA, LaFrance B, Zhang R, Kellogg EH, Westermann S, Rice LM, Nogales E. 2017 Structural differences between yeast and mammalian microtubules revealed by cryo-EM. *J. Cell Biol.* **216**, 2669–2677. (doi:10.1083/jcb.201612195)
66. McIntosh JR, O'Toole E, Zhudenkov K, Morphew M, Schwartz C, Ataullakhanov FI, Grishchuk EL. 2013 Conserved and divergent features of kinetochores and spindle microtubule ends from five species. *J. Cell Biol.* **200**, 459–474. (doi:10.1083/jcb.201209154)
67. Huang PS, Ban YE, Richter F, Andre I, Vernon R, Schief WR, Baker D. 2011 RosettaRemodel: a generalized framework for flexible backbone protein design. *PLoS ONE* **6**, e24109. (doi:10.1371/journal.pone.0024109)
68. Ramey VH, Wang HW, Nakajima Y, Wong A, Liu J, Drubin D, Barnes G, Nogales E. 2011 The Dam1 ring binds to the E-hook of tubulin and diffuses along the microtubule. *Mol. Biol. Cell.* **22**, 457–466. (doi:10.1091/mbc.E10-10-0841)
69. Afonine PV, Poon BK, Read RJ, Sobolev OV, Terwilliger TC, Urzhumtsev A, Adams PD. 2018 Real-space refinement in PHENIX for cryo-EM and crystallography. *Acta Crystallogr. D Struct. Biol.* **74**, 531–544. (doi:10.1107/S2059798318006551)
70. Wang Y *et al*. 2012 Coiled-coil networking shapes cell molecular machinery. *Mol. Biol. Cell.* **23**, 3911–3922. (doi:10.1091/mbc.E12-05-0396)
71. van Zundert GCP *et al*. 2016 The HADDOCK2.2 web server: user-friendly integrative modeling of biomolecular complexes. *J. Mol. Biol.* **428**, 720–725. (doi:10.1016/j.jmb.2015.09.014)
72. Zahm JA, Jenni S, Harrison SC. 2023 Structure of the Ndc80 complex and its interactions at the yeast kinetochore–microtubule interface. Figshare. (doi:10.6084/m9.figshare.c.6431801)